


Monitoring the Applied Strain in Monolayer Gallium Selenide through Vibrational Spectroscopies: A First-Principles Investigation

R. Longuinhos* and J. Ribeiro-Soares

Departamento de Física, Universidade Federal de Lavras, PO Box 3037, Lavras, Minas Gerais 37200-000, Brazil

 (Received 7 September 2018; revised manuscript received 24 November 2018; published 5 February 2019)

Monolayer gallium selenide (GaSe) is a promising material for nanoscale electronic, spintronic, and optoelectronic applications. Its electrical conductivity and optical properties were reported to be largely tuned by strain engineering, where the assessment of the applied strain is crucial. In this work, we apply first-principles calculations to unveil the strain-induced phonon frequency shifts in monolayer GaSe, showing its promising application as a strain probe. Furthermore, we find that the uniaxial-, biaxial-, and shear-strain onset for strain-induced lattice instability are 22%, 16%, and 5%, respectively, indicating it could be used as a handle in flexible electronics. We find monolayer GaSe to be about 2 times softer than monolayer MoS₂ and 4 times softer than monolayer graphene, and that its Raman fingerprint modes can resolve strain values in the low-strain regime up to 1.0%. These results suggest its use as a strain sensor in fragile applications. Our results provide insight into the use of Raman and infrared spectroscopies to probe the strain in monolayer GaSe, which is of paramount importance for further developments in strain engineering and flexible electronics in GaSe-based devices.

DOI: [10.1103/PhysRevApplied.11.024012](https://doi.org/10.1103/PhysRevApplied.11.024012)

I. INTRODUCTION

The experimental realization of two-dimensional (2D) materials [1–3] paved the way for the conception of flexible nanoelectronic devices [4]. Few-layer group-III monochalcogenides (MX , where $M = \text{Ga}$ or In and $X = \text{S}$ or Se) are a promising beyond-graphene materials family for nano-optoelectronics [5]. Experiments indicate that the band gap of gallium selenide (GaSe) can be tuned by control of the number of layers, from an indirect gap of approximately 3.4 eV in monolayer GaSe [6–8] to a direct gap of 2.00–2.11 eV in its bulk counterpart [7,9–13]. Few-layer and monolayer GaSe display interesting physical properties for electronic [14], optoelectronic [6,8,12,15–20], nonlinear-optics [21,22], piezoelectric [23], and spintronic [24] applications. In particular, the Mexican-hat-like shape of the highest valence band of monolayer GaSe [25] results in a van Hove singularity, which is expected to allow strong exchange splitting in the valence-band maxima [24]. Recent angle-resolved-photoemission-spectroscopy measurements confirmed this inverted-sombrero shape [8,26] and the previously predicted spin-orbit-induced split in the low-lying energy valence state [25,27], which have important roles in the high-energy photoresponse of monolayer GaSe [6].

Strain engineering is an important technique to tune device physical properties, (e.g., optical band gap,

conductivity of electricity, and conductivity of heat) [28–30]. In multilayer GaSe, uniaxial strain redshifts its photoluminescence spectrum by approximately 50 meV up to 3.0% strain [7], and linearly reduces its resistance by $10^7 \Omega/\%$ up to 20% strain [31]. First-principles calculations using the hybrid functional of Heyd, Scuseria, and Ernzerhof (HSE06) show that the band gap in monolayer GaSe can be linearly tuned in the window of 2.7–1.5 eV by uniaxial strain ($-0.12 \text{ eV}/\%$), and in the window of 2.7–0.5 eV by biaxial strain ($-0.22 \text{ eV}/\%$ up to 10% strain) [7,32–34].

A strain field perturbs the crystal structure and may induce a frequency shift of the optically active vibrational modes of the crystal. Raman spectroscopy is a well-established technique to probe nanomaterial structures by accessing the crystal vibrational modes [35–38]. This technique has been successfully used to monitor strain in 2D nanomaterials such as monolayer graphene [39–41], monolayer MoS₂ [42–45], and phosphorene [46,47]. In addition, the natural or strain-induced anisotropy in the Raman response can be used to determine the sample crystallographic orientation with respect to the applied strain, as reported for monolayer phosphorene [47], monolayer graphene [39,40], and monolayer MoS₂ [42,43,48]. Infrared (IR) near-field microscopy has been successfully applied to map residual strain in polar and doped semiconductor crystals with nanoscale resolution, and is a promising technique [49]. To the best of our knowledge, there is no report on the use of Raman or IR spectroscopy

*raphael.lobato@dfi.ufla.br

to probe the lattice vibrations and their response to strain in monolayer or few-layer GaSe.

Here we investigate the influence of strain on the Raman-active and infrared-active vibrational modes of monolayer GaSe by using first-principles calculations. Monolayer GaSe can sustain 21% uniaxial strain, 15% biaxial strain, and 4.0% shear strain, meeting the required plasticity for use in flexible-electronics applications. We estimate the 2D Young's modulus (E^{2D}), Poisson's ratio, Grüneisen parameters, and shear deformation potentials of monolayer GaSe. The strain-induced frequency shift of its Raman fingerprints modes can be used to probe the applied strain. We find monolayer GaSe to be approximately 2 times softer than monolayer MoS₂ and approximately 4 times softer than monolayer graphene. These findings suggest that monolayer GaSe could be used as a strain sensor ideal for fragile applications. Under nonbiaxial strain, the doubly degenerate vibrational modes split into two modes; the atomic displacements of one mode are parallel to the pulling direction and those of the other mode are perpendicular to it. In the case of the lowest-energy optically active degenerate modes, the resulting nondegenerate mode with atomic displacements parallel to the pulling direction displays a strain-induced frequency blueshift, an unusual trend neither observed nor predicted to be displayed by monolayer MoS₂ or by monolayer graphene. This trend is understood by our analysis of the atomic quadrilayer structure of monolayer GaSe.

This paper is organized as follows. In Sec. II we describe the theoretical methods. In Sec. III A we discuss the geometry of monolayer GaSe and its vibrational modes under zero strain. Section III B 1 concerns the monolayer mechanical properties and strain-induced geometry deformations. In Sec. III B 2 we discuss the strain-induced phonon frequency shifts. Section IV summarizes the main conclusions on the influence of strain on the lattice dynamics and optically active vibrational modes of monolayer GaSe.

II. METHODS

We apply density-functional theory (DFT) [50,51] and density-functional perturbation theory (DFPT) [52,53] with 2D open-boundary conditions [53] by using the plane-wave self-consistent-field (PWSCF) and PHONON packages of the QUANTUM ESPRESSO distribution [54,55]. We use the Monkhorst-Pack scheme [56] to sample the Brillouin zone by using $8 \times 8 \times 1$ and $6 \times 8 \times 1$ Γ -centered grids for the primitive-cell and conventional-cell geometries, respectively. Forces on the atoms and stress on the lattice are lower than 0.01 mRy/bohr and 50 MPa, respectively. We simulate the uniaxial-stress condition along the zigzag and armchair directions by the optimization of both atomic positions and the in-plane lattice vector perpendicular to the strain field. The biaxial-stress condition is

simulated by imposing an isotropic deformation, while the imposed deformation in the case of pure shear stress preserves the in-plane area for small strain values (the strain components are given by $\epsilon_{xx} = -\epsilon_{yy}$). Phonon frequencies, infrared excitations, and Raman scattering are computed with the use of DFPT [53,57–59]. The exchange-correlation energy is evaluated within the Perdew-Zunger local-density approximation (LDA) [60]. The valence electron-ion interaction is described by use of a modified Bachelet-Hamann-Schulter scheme for norm-conserving pseudopotentials [61,62]. The plane-wave kinetic energy cutoff to describe the electronic wave functions (charge density) is set to 60 Ry (240 Ry). Phonon dispersions are calculated from the interatomic-force-constant matrix, obtained from dynamical matrices at phonon wave vectors in grids of $8 \times 8 \times 1$. The choices of paths in the Brillouin zone are based on the material's space group [63,64]. The names of the space groups are given according to the conventions in Ref. [65].

III. RESULTS AND DISCUSSION

A. Unstrained monolayer

Monolayer GaSe belongs to the D_{3h}^1 hexagonal space group. It can be represented by either primitive ($a = 3.690 \text{ \AA}$) or conventional [$\mathbf{a} = 6.391 \text{ \AA} \hat{x}$ (armchair), $\mathbf{b} = 3.690 \text{ \AA} \hat{y}$ (zigzag)] cells, shown in Fig. 1(a) by dotted and solid lines, respectively. We highlight in Fig. 1(b) the Ga—Ga ($l_{\text{Ga—Ga}} = 2.365 \text{ \AA}$) and Ga—Se ($l_{\text{Ga—Se}} = 2.423 \text{ \AA}$) bond lengths and the z component of the latter

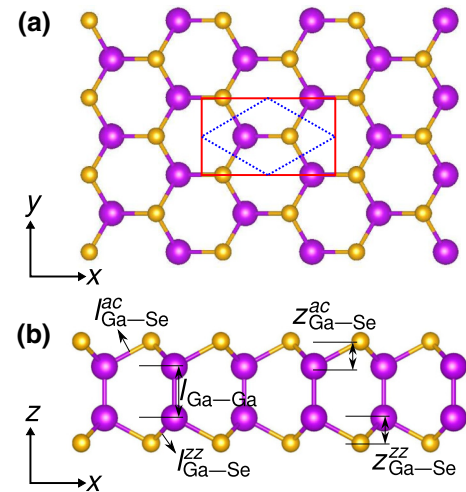


FIG. 1. Free monolayer GaSe. (a) Top view. (b) Side view. The Ga—Ga bond length and the Ga—Se bond length and the z component of the Ga—Se bond along the armchair and zigzag directions are indicated by $l_{\text{Ga—Ga}}$, $l_{\text{Ga—Se}}^{ac}$ and $z_{\text{Ga—Se}}^{ac}$, and $l_{\text{Ga—Se}}^{zz}$ and $z_{\text{Ga—Se}}^{zz}$, respectively. Primitive and conventional cells are drawn with dotted and solid lines, respectively. Gallium (selenium) atoms are represented as big purple (small orange) balls.

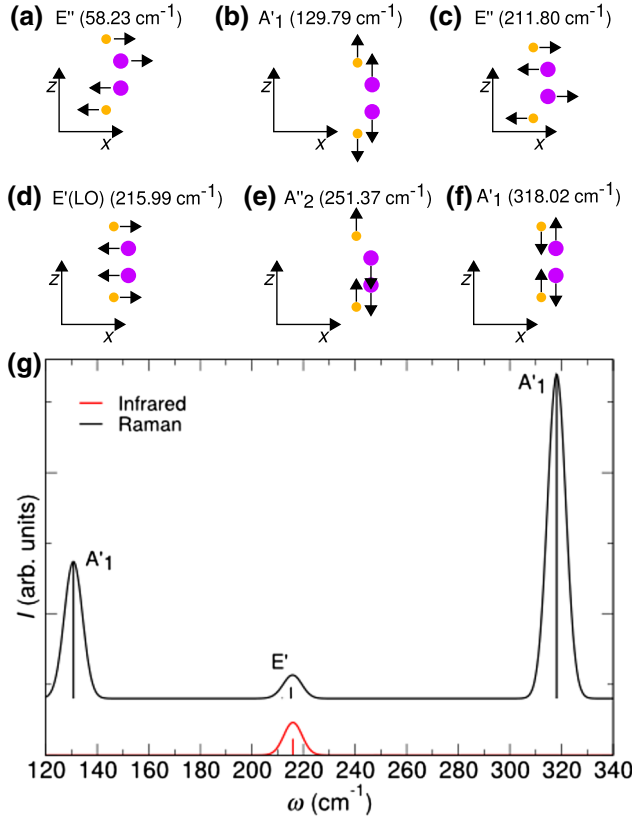


FIG. 2. Long-wavelength (Γ) optically active modes under zero strain. (a)–(f) Atomic displacement pattern and frequencies. Only one of the doubly degenerate E-type modes is shown (the other is orthogonal to it). (g) Raman and infrared spectra convoluted by use of Gaussian broadening.

($z_{\text{Ga—Se}} = 1.154 \text{ \AA}$). By their analysis, we obtain, for example, the monolayer thickness, $t = l_{\text{Ga—Ga}} + 2z_{\text{Ga—Se}}$.

Monolayer GaSe displays nine optically active modes, shown in Figs. 2(a)–2(f). The A'_1 and E' modes are predicted to be the Raman fingerprints, and the latter is also predicted to be an infrared fingerprint [see Fig. 2(g)]. To date, the E'' and A''_2 modes have not been reported in studies using Raman or infrared spectroscopy. The longitudinal optical (LO) and transverse optical (TO) E' modes are degenerate at Γ [57,66–69], as shown in Fig. 3, in agreement with previous LDA calculations [25]. Our results for the zone-center vibrational modes are in excellent agreement with recent measurements in encapsulated monolayer GaSe [13], further validating the use of the LDA. The frequencies of the low-frequency A'_1 and E' modes are underestimated by 4.4 cm^{-1} (3.3%) and overestimated by 1.5 cm^{-1} (0.7%), respectively, while the high-frequency A'_1 mode is overestimated by 7.7 cm^{-1} (2.5%).

The Raman spectrum of exposed monolayer GaSe [70,71] differs considerably from the spectrum of encapsulated samples [13]. On another hand, it is in good agreement with our results for the non-zone-center $E'(LO)$

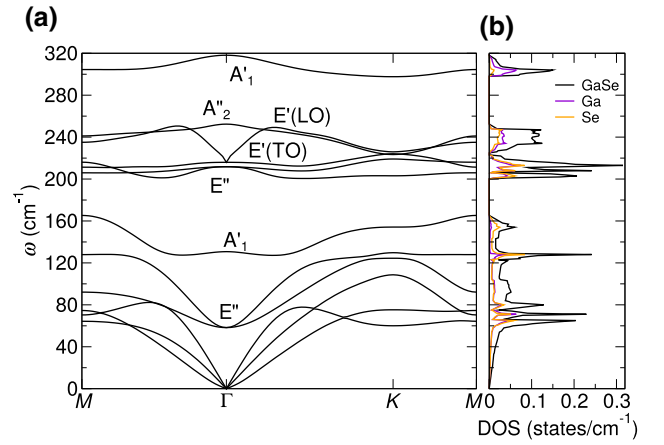


FIG. 3. Lattice vibrational structure under zero strain. (a) Phonon dispersion. The branches are labeled by their irreducible representation at Γ . (b) Phonon density of states (DOS). The total contribution and the contribution per atom of gallium and selenium are indicated by black, violet, and orange, respectively.

and the high-frequency A'_1 branches near Γ . Near Γ , the calculated frequency of the $E'(LO)$ mode is lower than the experimental frequency by 3.5 – 5.5 cm^{-1} (1.3%–2.1%), and the calculated frequency of the A'_1 mode exceeds the experimental frequency by 9.0 – 9.8 cm^{-1} (3.0%–3.3%) [70,71] (see Fig. 3 and Table I). Non-zone-center vibrational modes are observed in the presence of defects, which provide additional scattering processes that allow momentum conservation [35]. The broad Raman peak near 250 cm^{-1} , attributed to amorphous selenium, and the weak signal near 130 cm^{-1} are present in exposed ultrathin GaSe [72,73] and resemble the results reported for exposed monolayer GaSe [70,71]. In Table I we compare the phonon frequencies of the optically active modes with available experimental values obtained by Raman spectroscopy and previous LDA calculations.

B. Strained monolayer

1. Geometry deformation

Typical strain-engineering setups for 2D materials use a two-point or a four-point contact rig to apply uniaxial stress [40,44] and two three-point contact rigs to apply biaxial strain [74], these being some experimental strategies to be explored in monolayer GaSe. Under strain, monolayer GaSe suffers geometry deformations, which are fundamentally linked to the frequency of its vibrational modes. In this section, these geometric modifications are discussed to understand the trends observed in the phonon frequencies studied in the next section.

Under in-plane biaxial strain (b_{xy} from now on), the symmetries of monolayer GaSe are preserved. The stretched geometry in this situation resembles that of the free material, as presented in Fig. 1. Under uniaxial stress

TABLE I. Vibrational modes of unstrained monolayer GaSe. Our theoretical results are at Γ if not indicated otherwise. Experimental results are from Raman spectroscopy.

Mode	LDA (cm ⁻¹)		Experiment (cm ⁻¹)
	This work	Reference [13]	
E''	58.23	55.4	
A'_1	129.76	129.8	134.2 [13]
E''	211.80	211.6	
E' (TO)	215.99	217.0	214.5 [13]
E' (LO)	215.99, 249.25 ($\overline{\Gamma K}$), 250.54 ($\overline{\Gamma M}$)	217.0	214.5 [13], 254 [70], 256 [71]
A''_2	251.37	248.3	
A'_1	309.91 ($\overline{\Gamma K}$), 310.80 ($\overline{\Gamma M}$), 318.02	312.5	301 [70,71], 310.3 [13]

along the armchair, zigzag, and shear-strain directions (or ac , zz , and sxy , respectively, from now on), strain-induced symmetry lowering occurs. The monolayer threefold rotation axis along the \hat{z} direction and the in-plane twofold rotation axis are lost. These strained structures, shown in Fig. 4, possess the symmetry operations of the C_{2v}^{14} orthorhombic space group (no. 38). Under uniaxial stress (ac , zz), the crystal contracts transversely to the pulling axis by $\epsilon_{tt} = -\nu\epsilon_{ll}$, where ν is the Poisson's ratio, and ϵ_{ll} is the pulling strain. The Poisson's ratio is anisotropic for ac (ν_{ac}) and zz (ν_{zz}) strain (also predicted for monolayer graphene [75]), with average values up to 1.0% strain equal to $\bar{\nu}_{ac} = 0.23$ and $\bar{\nu}_{zz} = 0.29$ (see Fig. S1 in Supplemental Material [76]).

The strained geometry may become unstable due to phonon instabilities, resulting in structural breaking. The strain onsets for strain-induced lattice instability are approximately 16%, 5%, 22%, and 18% under bxy , sxy , ac , and zz strain, respectively (see Figs. S2 and S3 in Supplemental Material [76]). Recent reports have shown that GaSe nanosheets sustain up to 5% strain, applied by an

AFM tip [77], and multilayer wrinkled GaSe sustains 20% uniaxial strain, applied by a contact rig [31].

A general picture of the strain-induced deformations in monolayer GaSe is obtained by analyzing the deformations in the monolayer thickness t , bond length $l_{\text{Ga—Se}}$, and bond angle Θ (the angle formed by Se—Ga—Se along the armchair direction; see Fig. 4) up to 1.3% strain, as shown in Figs. 5(a)–5(c), respectively (see Fig. S4 in Supplemental Material [76] for the deformations in the monolayer $l_{\text{Ga—Ga}}$, $z_{\text{Ga—Se}}^{ac}$, and $z_{\text{Ga—Se}}^{zz}$). The monolayer thickness t does not change under sxy strain, while it shrinks linearly under bxy , ac , and zz strain. These reductions in t are mainly due to the changes in the atomic distance $z_{\text{Ga—Se}}$; the deformation of $l_{\text{Ga—Ga}}$ can be disregarded [see Fig. S4(a) in Supplemental Material [76]]. Under bxy strain, the bond length $l_{\text{Ga—Se}}$ and the bond angle Θ increase isotropically. Under ac strain, the bond lengths $l_{\text{Ga—Se}}^{ac}$ and $l_{\text{Ga—Se}}^{zz}$ increase and the bond angle Θ decreases, resulting in the expected Poisson contraction. While in the previous cases the overall effect is to increase both $l_{\text{Ga—Se}}^{ac}$ and $l_{\text{Ga—Se}}^{zz}$, under zz strain $l_{\text{Ga—Se}}^{ac}$ decreases, $l_{\text{Ga—Se}}^{zz}$ increases, and Θ increases. As a result, the crystal is reduced along the \hat{x} direction by $-\nu_{zz}\epsilon$. Under sxy strain, the bond length $l_{\text{Ga—Se}}^{ac}$ increases and $l_{\text{Ga—Se}}^{zz}$ is reduced, similarly to the case under zz strain, and Θ decreases, similarly to the case under ac strain.

We may estimate the stress necessary to strain the monolayer in experiments by rescaling the *supercell stress* σ [78–80] into the *equivalent stress* $\sigma^{\text{eqv}} = \sigma \times c/t$ [75], where c is the supercell height (18 Å in our case) and t is the monolayer thickness. Stresses of 2.7, 1.8, 2.2, and 2.1 GPa cause 1.3% bxy , sxy , ac , and zz strain, respectively [see Fig. S5(a) in Supplemental Material [76]]. These values, which represent a feasible load, may be considered upper boundary values, as the LDA overestimates the cohesion energy and underestimates lattice constants.

The in-plane elastic stiffness in 2D materials (2D Young's modulus) is given by $E^{2D} = 1/A_0 \partial^2 E / \partial \epsilon_{bxy}^2$ [33], where A_0 is the equilibrium in-plane area and E is the energy under bxy strain (ϵ_{bxy}). For monolayer GaSe we find $E^{2D} = 96$ N/m [see Fig. S5(b) in Supplemental

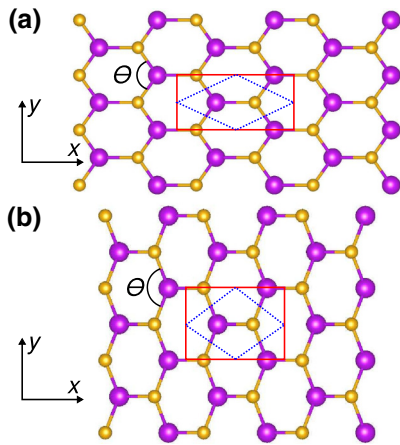


FIG. 4. Strained geometries. (a) ac strain; similar to the sxy -strain case. (b) zz strain. Primitive and conventional cells are drawn with dotted and solid lines, respectively. The angle Θ formed by Se—Ga—Se along the zigzag direction is highlighted.

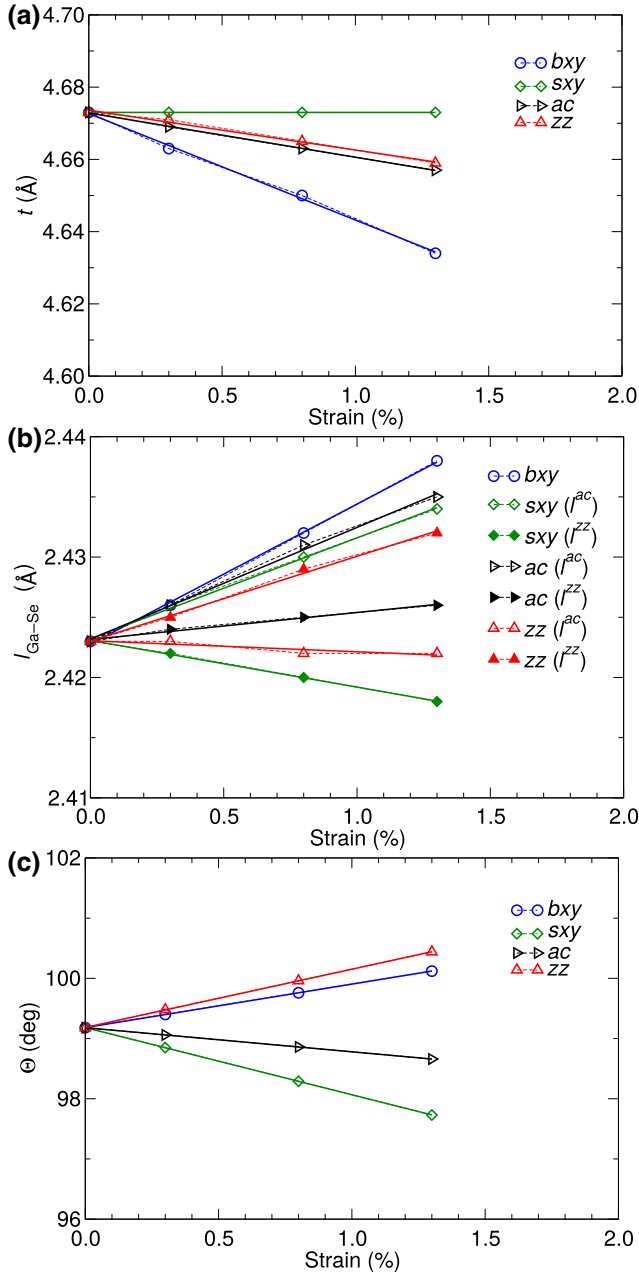


FIG. 5. Structural deformations under bxy (circles), sxy (diamonds), ac (rightward-pointing triangles), and zz (upright triangles) strain. (a) Thickness t . (b) Ga—Se bond length $l_{\text{Ga—Se}}$; open and filled symbols represent $l_{\text{Ga—Se}}^{ac}$ and $l_{\text{Ga—Se}}^{zz}$, respectively. (c) Se—Ga—Se angle Θ .

Material [76]], in good agreement with previous theoretical reports [23,32,33,81]. This value is 1.87 times smaller than that for monolayer MoS_2 and 4.05 times smaller than that for monolayer graphene. This trend is in agreement with the findings in previous experiments in GaSe nanosheets [77], monolayer MoS_2 [82], and monolayer graphene [83]. These results, summarized in Table II, indicate that monolayer GaSe is the softest among these materials. This adds to recent predictions that GaSe is

a better lubricant than MoS_2 and as good a lubricant as graphite [84].

2. Phonon frequency shifts

The strain induces perturbation of the crystal structure and, consequently, the atomic orbital interactions are affected. This may result in frequency shift of the material vibrational modes. For example, it is reasonable to expect a greater vibrational frequency shift rate under bxy strain, where greater and isotropic elongation of the Ga—Se bonds occurs in comparison with ac , zz , and sxy strain [see Fig. 5(b)]. Also, one expects that the vibrations of bonds with atomic displacements parallel to the strain become softer under tensile strain and harder under compression in comparison with the free condition. The aim of this section is to obtain detailed understanding of phonon frequency shifts due to specific strain.

The strain-induced phonon frequency shift $\partial\omega_i$ at the frequency of the i th nondegenerate vibrational mode ω_i^0 due to a bxy strain (ϵ_{bxy}) may be understood in terms of its Grüneisen parameter γ_i [40,44,85]:

$$\gamma_i = -\frac{1}{2\omega_i^0} \frac{\partial\omega_i}{\partial\epsilon_{bxy}}. \quad (1)$$

Under sxy strain (ϵ_{sxy}), $\partial\omega_i$ may be understood in terms of its shear deformation potential β_i [40,44,85,86]:

$$\beta_i = -\frac{1}{2\omega_i^0} \frac{\partial\omega_i}{\partial\epsilon_{sxy}}. \quad (2)$$

The strain evolution of the in-plane doubly degenerate modes of monolayer GaSe is given by [35,39,40,86–88]

$$\frac{\Delta\omega_i^\pm}{\omega_i^0} = -\gamma_i\epsilon_h \pm \frac{1}{2}\beta_i\epsilon_s, \quad (3)$$

where $\epsilon_h = \epsilon_{xx} + \epsilon_{yy}$ and $\epsilon_s = \epsilon_{xx} - \epsilon_{yy}$ [here ϵ_{xx} and ϵ_{yy} are strain components along the armchair (\hat{x}) and zigzag (\hat{y}) directions, respectively].

Under bxy strain, symmetry breaking does not occur, there is thus no degeneracy lift, and $\Delta\omega_i$ can be expressed as

$$\Delta\omega_i = -2\omega_i^0\gamma_i\epsilon_{bxy}. \quad (4)$$

Under ac , zz , and sxy strain, symmetry breaking is expected, and the doubly degenerate modes split into two nondegenerate modes. Under sxy strain, $\Delta\omega_i$ evolves as

$$\Delta\omega_i^\pm = \pm\omega_i^0\beta_i\epsilon_{sxy}, \quad (5)$$

and under ac and zz strain, $\Delta\omega_i$ evolves as

$$\Delta\omega_i^\pm = \omega_i^0 \left[-\gamma_i(1-\nu) \pm \frac{1}{2}\beta_i(1+\nu) \right] \epsilon, \quad (6)$$

TABLE II. Two-dimensional Young's modulus E^{2D} of monolayer GaSe and other 2D materials. Calculated values in this work are obtained by use of the Perdew-Zunger LDA. Calculated values from others theoretical studies obtained by use of the Perdew-Burke-Ernzerhof generalized-gradient approximation (GGA) and the Heyd-Scuseria-Ernzerhof hybrid functional (HSE06) are included. The experimental value for monolayer GaSe is estimated from the reported value for GaSe nanosheets (by use of $E^{3D} = E^{2D}/h$, where h is the interlayer spacing in bulk GaSe and E^{3D} is its Young's modulus).

	E^{2D} (N/m)			
	Experiment	GGA	LDA	HSE06
Monolayer GaSe	66 ± 10 [77]	66 [23], 67 [81], 67 [32], 79 [33]	96	104 [33]
Monolayer MoS ₂	180 ± 60 [82]	160 [44], 165 [33]	180	189 [33]
Monolayer graphene	340 ± 50 [83]		390	

where ϵ is the pulling strain and ν is the in-plane Poisson's ratio. From these, γ_i and β_i are expressed as

$$\beta_i = \frac{\Delta\omega_i^+ - \Delta\omega_i^-}{\omega_i^0(1+\nu)\epsilon}, \quad \gamma_i = \frac{\Delta\omega_i^+ + \Delta\omega_i^-}{2\omega_i^0(1-\nu)\epsilon}. \quad (7)$$

In the case of a suspended monolayer, its own ν should be used (e.g., $\bar{\nu}_{ac}$ or $\bar{\nu}_{zz}$ under ac or zz strain, respectively). When a substrate is used to transfer strain to the monolayer (raising discussions about the effective strain transferred [41]), ν of the substrate is normally used. Under

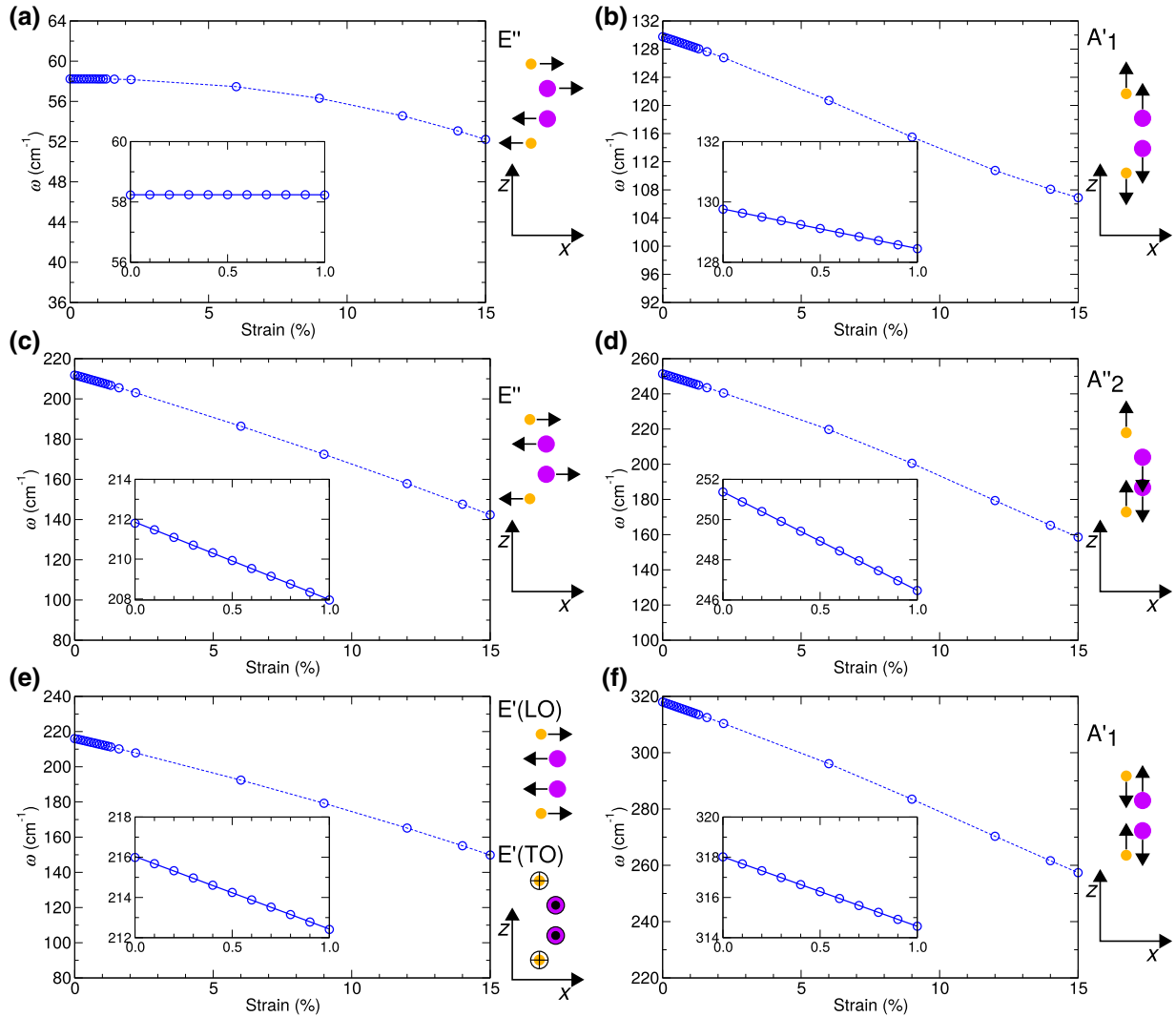


FIG. 6. (a)–(f) Phonon frequency shift under bxy strain. Dashed lines are a guide for the eye for the DFT calculations (circles). The insets show a linear fit (solid line) of the DFT results up to 1.0% strain. At the side of the plots, the phonon's atomic displacement patterns are shown and its irreducible representations are indicated.

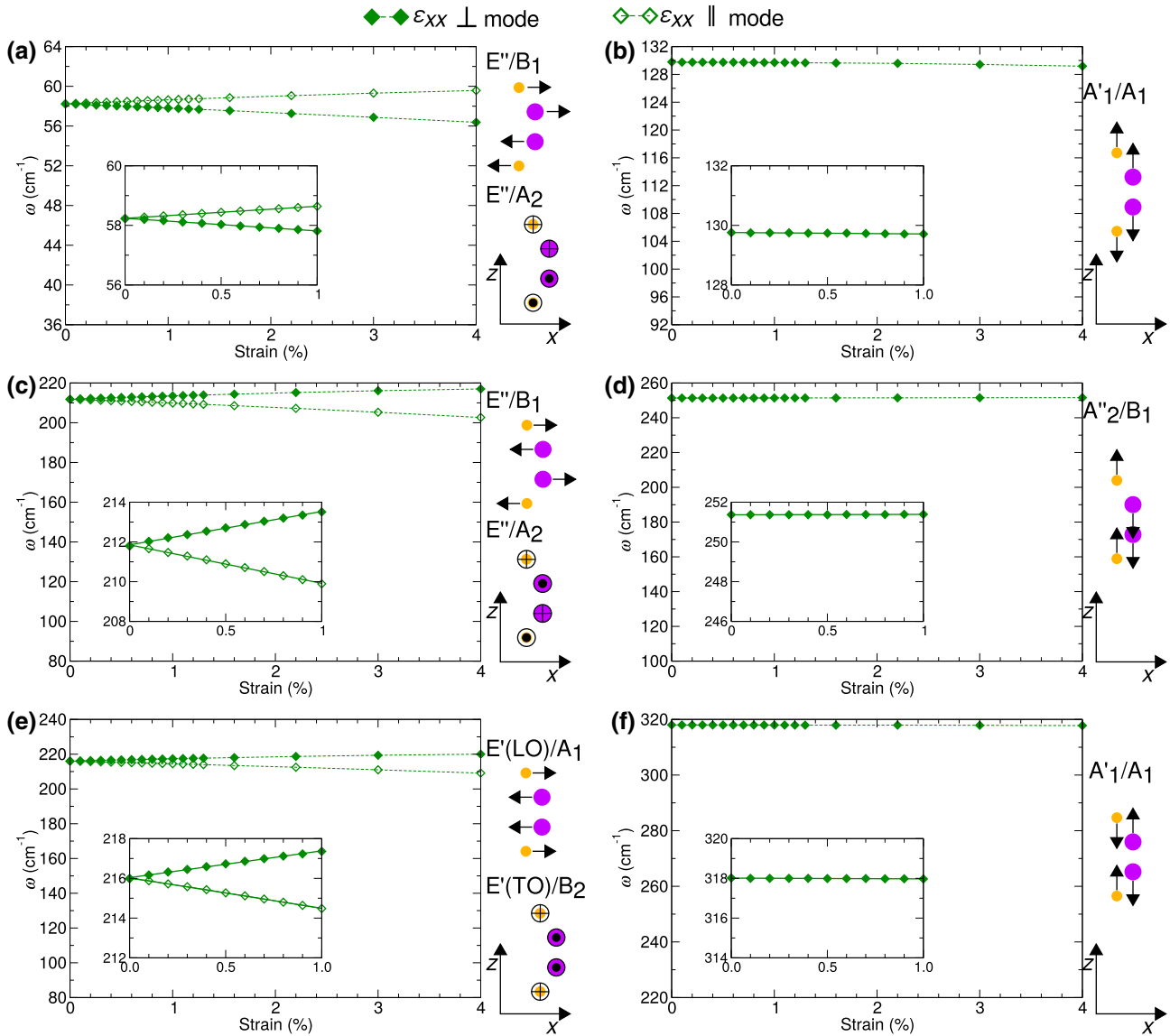


FIG. 7. (a)–(f) Phonon frequency shift under sxy strain. Dashed lines are a guide for the eye for the DFT calculations (diamonds). Modes with an atomic displacement pattern parallel to the ϵ_{xx} strain are represented by open symbols and modes with an atomic displacement pattern perpendicular to the ϵ_{xx} strain are represented by filled symbols. The insets show a linear fit (solid line) of the DFT results up to 1.0% strain. At the side of each plot, the phonon’s atomic displacement patterns are shown and its irreducible representations before and after (separated by a slash) the deformation are indicated.

bxy or sxy strain, $\Delta\omega_i$ is independent of the Poisson’s ratio of both monolayer GaSe and the substrate. This is a specially important result for monolayer GaSe given that its band gap is expected to be tunable in the wide range of 2.7 to 0.5 eV up to 10% bxy strain [7,32–34].

In Figs. 6 and 7 we present the evolution of the optically active modes under bxy and sxy strain, respectively. In Fig. 8 we present the evolution of the optically active modes under uniaxial ac - and zz -stress conditions. In these figures, dashed lines are a guide for the eye for the DFT results (symbols). In the inset, solid lines are the linear fit of these results considering strain values up to 1.0%. At the right of the plots we give the atomic displacement

pattern of the related vibrational mode. From these results, we obtain $\Delta\omega_i/\epsilon$, γ_i , and β_i of the modes presented in Table III.

In general, the vibrational modes of monolayer GaSe display strain-induced phonon frequency shifts $\Delta\omega_i/\epsilon$ lower than or comparable to the reported values for monolayer MoS₂ [43,44], and at least 10 times smaller than the reported values for monolayer graphene [40,41,89]. These results are in agreement with our previous discussion on the mechanical properties of monolayer GaSe, which is softer than monolayer MoS₂ and monolayer graphene.

The Grüneisen parameters of monolayer GaSe are lower than or comparable to the reported values for monolayer

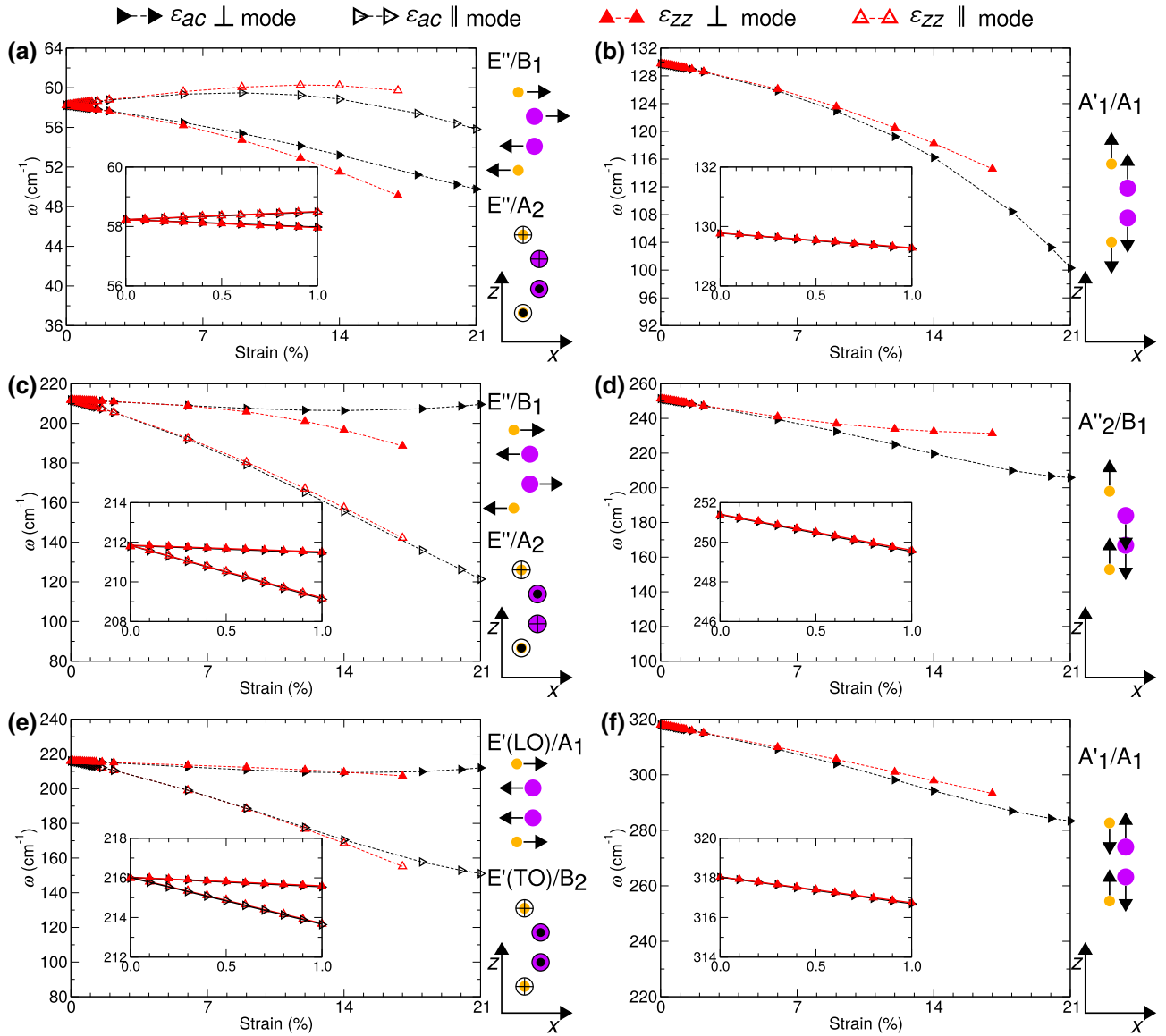


FIG. 8. Phonon frequency shift under ac and zz strains. Dashed lines are a guide for the eye for the DFT calculations (ac and zz are represented by rightward-pointing triangles and upright triangles, respectively). Modes with an atomic displacement pattern parallel to the strain are represented by open symbols and modes with an atomic displacement pattern perpendicular to the strain are represented by filled symbols. The insets show a linear fit (solid line) of the DFT results up to 1.0% strain. At the side of each plot, the phonon's atomic displacement patterns are shown and its irreducible representations before and after (separated by a slash) the deformation are indicated.

MoS₂ [43,44] and at least 0.5 times lower than the reported values for monolayer graphene [40,41,89]. As a result, the monolayer-GaSe Raman fingerprint modes of type A' and E' display strain-induced phonon frequency shifts sufficiently large to be used to probe small strain (e.g., below 1.0% strain), with the exception of the A' modes when the monolayer is under s_{xy} strain. As monolayer GaSe is soft, we suggest its use as a strain sensor ideal for fragile applications.

The Se—Ga—Ga—Se atomic quadrilayer structure of monolayer GaSe allows two doubly degenerate phonon atomic displacement patterns, where the Ga—Se bonds are

rigid and the Ga—Ga bond stretches in the xy plane. These E'' modes are the lowest-energy optically active vibrational modes of monolayer GaSe. They display zero $\Delta\omega_{E''}$ in the case of small b_{xy} strain [see Fig. 6(a)], which is reasonable if it is taken into account that the b_{xy} strain causes an isotropic expansion, and a very small increase of the bond length $l_{\text{Ga—Ga}}$ only for large strain values. Zero $\Delta\omega_{E''}$ in this case implies zero $\gamma_{E''}$. This result indicates that these long-wavelength vibrations are not important for strain monitoring, and also do not contribute to the thermal lattice expansion in the linear regime [90]. These modes get harder under a tensile strain parallel to them in addition

TABLE III. Phonon frequency shifts ($\Delta\omega$), Grüneisen parameter (γ), and shear deformation potential (β) for the Raman-active and infrared-active modes of monolayer GaSe under ac , zz , bxy , and sxy strain. The irreducible representation of the mode before (after) deformation is indicated. Under bxy , strain symmetry breaking does not occur.

Irreducible representation	$\Delta\omega/\epsilon$ (cm ⁻¹ /% strain)			γ			β			
	bxy	sxy	ac	zz	bxy	ac	zz	sxy	ac	zz
E'' (A_2 , B_1)	0.000(4)	-0.425(4), 0.405(2)	-0.250(3), +0.256(4)	+0.269(4), -0.265(3)	0.000	0.007	0.006	0.712	0.705	0.711
A_1' (A_1)	-1.311(6)	-0.049(5)	-0.512(7)	-0.499(9)	0.505			0.019		
E'' (A_2 , B_1)	-3.882(22)	1.680(23), -1.932(23)	-0.364(15), -2.695(19)	-2.656(21), -0.337(21)	0.916	0.941	0.994	0.853	0.893	0.850
E' (TO, LO) (B_2 , A_1)	-3.606(19)	1.350(21), -1.529(15)	-0.470(12), -2.354(11)	-2.336(21), -0.435(16)	0.835	0.852	0.902	0.666	0.707	0.682
A_2'' (B_1)	-4.900(5)	0.022(4)	-1.865(10)	-1.818(18)	0.975			-0.004		
A_1' (A_1)	-3.452(3)	-0.022(5)	-1.345(9)	-1.310(13)	0.543			0.006		

to a compressive strain perpendicular to them [e.g., under sxy strain; open diamonds in Fig. 7(a)], or under a pulling strain parallel to them [e.g., under ac strain and zz strain; open right-pointing triangles and open upright triangles, respectively, in Fig. 8(a)].

To understand the unusual strain-induced phonon-frequency shift of the lowest-energy E'' mode, we compute the total energy variation $\delta E_i = E(\delta\mathbf{r}) - E(\mathbf{r}_0)$ due to the displacement of the atoms in the strained geometry by $\delta\mathbf{r}$, according to the phonon atomic displacement of the i th mode from its equilibrium position \mathbf{r}_0 . Under nonbiaxial strain, the doubly degenerate E'' modes splits in two, one A_2 mode and one B_1 mode. Under ac strain, the A_2 mode is perpendicular to the strain field and becomes softer, while the B_1 mode is parallel to the strain field and becomes harder [filled and open rightward-pointing triangles, respectively, in Fig. 8(a)]. In this case, $\delta\mathbf{r} = 0.1$ Å results in $\delta E_{B_1} - \delta E_{A_2} = 0.8$ meV, and $\delta\mathbf{r} = 0.2$ Å results in $\delta E_{B_1} - \delta E_{A_2} = 3.31$ meV. These trends indicate that the geometry deformation related to the A_2 mode in the ac -strained structure causes lower internal restoring forces in comparison with the deformation related to the B_1 mode. Similar arguments can be applied to the cases under sxy and zz strains, with the overall effect resulting in the unconventional strain dependence of these E'' modes.

The remaining doubly degenerate modes display the expected strain dependence, where the atomic vibration with components (i) along the tensile-strain direction becomes softer than under zero strain, (ii) perpendicular to the tensile strain become less soft than under zero strain, and (iii) along the compressive-strain direction becomes harder than under zero strain. For example, the E'' mode at 211 cm⁻¹ splits into one A_2 mode and one B_1 mode when the monolayer is under ac and zz strains, as shown in Fig. 8(c). The frequencies of the atomic vibrations with displacement patterns parallel or perpendicular to the strain field are represented by open or filled symbols. Under ac strain (rightward-pointing triangles), the B_1 vibration

pattern is parallel to the pulling strain and becomes softer than the A_2 mode, which is perpendicular to it. Under zz strain (upright triangles), the B_1 vibration pattern is perpendicular to the strain field and becomes less soft than the A_2 mode, which is now parallel to the strain field.

IV. CONCLUSION

In this work, we use first-principles calculations to unveil the strain-induced mechanical deformation and phonon frequency shifts of the Raman-active and infrared-active vibrational modes in monolayer GaSe. We estimate important mechanical and thermodynamic parameters, as its 2D Young's modulus, Poisson's ratio, Grüneisen parameters, and shear deformation potentials. We find that monolayer GaSe is approximately 2 times softer than monolayer MoS₂ and approximately 4 times softer than monolayer graphene. The Raman fingerprint E' and A_1' modes display strain-induced phonon frequency shifts that may be used to probe applied strain smaller than 1.0%. These results suggest the use of Raman spectroscopy to probe the applied strain in monolayer GaSe, and the use of this material as a strain sensor for fragile applications. Because of the atomic quadrilayer structure of monolayer GaSe, its lowest-frequency E'' modes display an unusual strain-induced frequency shift, becoming harder when their atomic vibration displacement pattern is parallel to the tensile strain. Furthermore, we find that monolayer GaSe can sustain uniaxial strain as large as 21%, biaxial strain as large as 15%, and pure shear strain as large as 4%, large enough for applications in flexible electronics. Our results provide insight into the lattice dynamics of strained monolayer GaSe and the expected trends for the use of Raman and infrared spectroscopies to probe the applied strain on it, crucial information for the realization of flexible electronics and strain-engineering enhancements in microelectronics based on this beyond-graphene 2D material.

ACKNOWLEDGMENTS

We thank the Brazilian National Council for Scientific and Technological Development (CNPq; Grants No. 310813/2017-4, No. 433027/2018-5, and No. 420364/2018-8), Foundation for Research Support of Minas Gerais (Fapemig; Grants No. CEX-APQ-02136-15, No. CEX-APQ-01865-17, No. APQ-01980-18, No. TEC-AUC-00026-16, No. RED-00185-16, and No. RED-00282-16), and Agency for Financing Studies and Projects [FINEP; Grants No. 0058/16 (DMOL), No. 0501/16 (NANO) from FINEP 02/2014, and FINEP 02/2016]. R.L. acknowledges computational time at CENAPAD-SP, CENAPAD-RJ/LNCC, DFI-UFLA, and LCC-UFLA. J.R.-S. acknowledges support from the Pró-Reitoria de Pesquisa and Pró-Reitoria de Gestão (UFLA) and the L'Oréal-UNESCO–Academia Brasileira de Ciências *Prêmio Para Mulheres na Ciência* (Prize for Women in Science; Brazil, 2017).

-
- [1] K. S. Novoselov, A. K. Geim, S. V. Morozov, D. Jiang, Y. Zhang, S. V. Dubonos, I. V. Grigorieva, and A. A. Firsov, Electric field effect in atomically thin carbon films, *Science* **306**, 666 (2004).
- [2] Willi Auwärter, Hans Ulrich Suter, Hermann Sachdev, and Thomas Greber, Synthesis of one monolayer of hexagonal boron nitride on Ni(111) from B-trichloroborazine (CIBNH)₃, *Chem. Mater.* **16**, 343 (2004).
- [3] K. S. Novoselov, D. Jiang, F. Schedin, T. J. Booth, V. V. Khotkevich, S. V. Morozov, and A. K. Geim, Two-dimensional atomic crystals, *Proc. Natl. Acad. Sci. USA* **102**, 10451 (2005).
- [4] Gianluca Fiori, Francesco Bonaccorso, Giuseppe Iannaccone, Tomas Palacios, Daniel Neumaier, Alan Seabaugh, Sanjay K. Banerjee, and Luigi Colombo, Electronics based on two-dimensional materials, *Nat. Nano* **9**, 768 (2014).
- [5] Wenjuan Huang, Lin Gan, Huiqiao Li, Ying Ma, and Tianyou Zhai, 2S layered group IIIA metal chalcogenides: Synthesis, properties and applications in electronics and optoelectronics, *Cryst. Eng. Comm.* **18**, 3968 (2016).
- [6] Sidong Lei, Liehui Ge, Zheng Liu, Sina Najmaei, Gang Shi, Ge You, Jun Lou, Robert Vajtai, and Pulickel M. Ajayan, Synthesis and photoresponse of large GaSe atomic layers, *Nano Lett.* **13**, 2777 (2013).
- [7] Chan Su Jung, Fazel Shojaei, Kidong Park, Jin Young Oh, Hyung Soon Im, Dong Myung Jang, Jeunghye Park, and Hong Seok Kang, Red-to-ultraviolet emission tuning of two-dimensional gallium sulfide/selenide, *ACS Nano* **9**, 9585 (2015).
- [8] Zeineb Ben Aziza, Debora Pierucci, Hugo Henck, Mathieu G. Silly, Christophe David, Mina Yoon, Fausto Sirotti, Kai Xiao, Mahmoud Eddrief, Jean-Christophe Girard, and Abdelkarim Ouerghi, Tunable quasiparticleband gap in few-layergase/graphene van der Waals heterostructures, *Phys. Rev. B* **96**, 035407 (2017).
- [9] E. Aulich, J. L. Brebner, and E. Mooser, Indirect energy gap in GaSe and GaS, *Phys. Status Solidi (B)* **31**, 129 (1969).
- [10] A. Mercier, E. Mooser, and J. P. Voitchovsky, Resonant exciton in GaSe, *Phys. Rev. B* **12**, 4307 (1975).
- [11] Vito Capozzi, and Maurizio Montagna, Optical spectroscopy of extrinsic recombinations in gallium selenide, *Phys. Rev. B* **40**, 3182 (1989).
- [12] P. A. Hu, Z. Wen, L. Wang, P. Tan, and K. Xiao, Synthesis of few-layer GaSe nanosheets for high performance photodetectors, *ACS Nano* **6**, 5988 (2012).
- [13] Daniel J. Terry, Viktor Zólyomi, Matthew Hamer, Anastasia V. Tyurmina, David G. Hopkinson, Alexander Rakowski, Samuel J. Magorrian, Nick Clark, Yuri M. Andreev, Olga Kazakova, Konstantin Novoselov, Sarah J. Haigh, Vladimir I. Falko, and Roman Gorbachev, Infrared-to-violet tunable optical activity in atomic films of GaSe, InSe, and their heterostructures, *2D Mater.* **5**, 041009 (2018).
- [14] D. J. Late, B. Liu, J. Luo, A. Yan, H. S. S. Matte, M. Grayson, C. N. R. Rao, and V. P. Dravid, GaS and GaSe ultrathin layer transistors, *Adv. Mater.* **24**, 3549 (2012).
- [15] Yubing Zhou, Yufeng Nie, Yujing Liu, Kai Yan, Jinhua Hong, Chuanhong Jin, Yu Zhou, Jianbo Yin, Zhongfan Liu, and Hailin Peng, Epitaxy and photoresponse of two-dimensional GaSe crystals on flexible transparent mica sheets, *ACS Nano* **8**, 1485 (2014).
- [16] Xufan Li, Ming-Wei Lin, Alexander A. Puzos, Juan C. Idrobo, Cheng Ma, Miaofang Chi, Mina Yoon, Christopher M. Rouleau, Ivan I. Kravchenko, David B. Geohegan, and Kai Xiao, Controlled vapor phase growth of single crystalline, two-dimensional GaSe crystals with high photoresponse, *Sci. Rep.* **4**, 05497 (2014).
- [17] O. Del Pozo-Zamudio, S. Schwarz, M. Sich, I. A. Akimov, M. Bayer, R. C. Schofield, E. A. Chekhovich, B. J. Robinson, N. D. Kay, O. V. Kolosov, A. I. Dmitriev, G. V. Lashkarev, D. N. Borisenko, N. N. Kolesnikov, and A. I. Tartakovskii, Photoluminescence of two-dimensional GaTe and GaSe films, *2D Mater.* **2**, 035010 (2015).
- [18] Hai Huang, Peng Wang, Yanqing Gao, Xudong Wang, Tie Lin, Jianlu Wang, Lei Liao, Jinglan Sun, Xiangjian Meng, Zhiming Huang, Xiaoshuang Chen, and Junhao Chu, Highly sensitive phototransistor based on GaSe nanosheets, *Appl. Phys. Lett.* **107**, 143112 (2015).
- [19] Pil Ju Ko, Abdelkader Abderrahmane, Tsukasa Takamura, Nam-Hoon Kim, and Adarsh Sandhu, Thickness dependence on the optoelectronic properties of multilayered GaSe based photodetector, *Nanotechnology* **27**, 325202 (2016).
- [20] Abdelkader Abderrahmane, Pan-Gum Jung, Nam-Hoon Kim, Pil Ju Ko, and Adarsh Sandhu, Gate-tunable optoelectronic properties of a nano-layered GaSe photodetector, *Opt. Mater. Express* **7**, 587 (2017).
- [21] Xu Zhou, Jingxin Cheng, Yubing Zhou, Ting Cao, Hao Hong, Zhimin Liao, Shiwei Wu, Hailin Peng, Kaihui Liu, and Dapeng Yu, Strong second-harmonic generation in atomic layered GaSe, *J. Am. Chem. Soc.* **137**, 7994 (2015).
- [22] L. Karvonen, A. Säynätjoki, S. Mehravar, R. D. Rodriguez, S. Hartmann, D. R. T. Zahn, S. Honkanen, R. A. Norwood, N. Peyghambarian, K. Kieu, H. Lipsanen, and J. Riikonen, Investigation of second-and third-harmonic generation in few-layer gallium selenide by multiphoton microscopy, *Sci. Rep.* **5**, 10334 (2015).

- [23] Wenbin Li, and Ju Li, Piezoelectricity in two-dimensional group-III monochalcogenides, *Nano Res.* **8**, 3796 (2015).
- [24] Ting Cao, Zhenglu Li, and Steven G. Louie, Tunable magnetism and half-metallicity in hole-doped monolayer GaSe, *Phys. Rev. Lett.* **114**, 236602 (2015).
- [25] V. Zólyomi, N. D. Drummond, and V. I. Fal'ko, Band structure and optical transitions in atomic layers of hexagonal gallium chalcogenides, *Phys. Rev. B* **87**, 195403 (2013).
- [26] Zeineb Ben Aziza, Viktor Zólyomi, Hugo Henck, Debora Pierucci, Mathieu G. Silly, Julien Chaste, Chaoyu Chen, Mina Yoon, Kai Xiao, Fausto Sirotti, Maria C. Asensio, Emmanuel Lhuillier, Mahmoud Eddrief, Vladimir I. Fal'ko, and Abdelkarim Ouerghi, Valence band inversion and spin-orbit effects in the electronic structure of monolayer GaSe, *Phys. Rev. B* **98**, 115405 (2018).
- [27] Pengke Li, and Ian Appelbaum, Symmetry, distorted band structure, and spin-orbit coupling of group-III metal-monochalcogenide monolayers, *Phys. Rev. B* **92**, 195129 (2015).
- [28] M. A. Bissett, M. Tsuji, and H. Ago, Strain engineering the properties of graphene and other two-dimensional crystals, *Phys. Chem. Chem. Phys.* **16**, 11124 (2014).
- [29] Rafael Roldán, and Francisco Guinea, Strain engineering in semiconducting two-dimensional crystals, *J. Phys.: Condens. Matter* **27**, 313201 (2015).
- [30] Zhiyong Zhu, Yingchun Cheng, and Udo Schwingenschlögl, Topological phase transition in layered GaS and GaSe, *Phys. Rev. Lett.* **108**, 266805 (2012).
- [31] Cong Wang, Sheng-Xue Yang, Hao-Ran Zhang, Le-Na Du, Lei Wang, Feng-You Yang, Xin-Zheng Zhang, and Qian Liu, Synthesis of atomically thin GaSe wrinkles for strain sensors, *Front. Phys.* **11**, 116802 (2016).
- [32] Le Huang, Zhanghui Chen, and Jingbo Li, Effects of strain on the band gap and effective mass in two-dimensional monolayer GaX ($X = S, Se, Te$), *RSC Adv.* **5**, 5788 (2015).
- [33] Houlong L. Zhuang, and Richard G. Hennig, Single-layer group-III monochalcogenide photocatalysts for water splitting, *Chem. Mater.* **25**, 3232 (2013).
- [34] Yandong Ma, Ying Dai, Meng Guo, Lin Yu, and Baibiao Huang, Tunable electronic and dielectric behavior of GaS and GaSe monolayers, *Phys. Chem. Chem. Phys.* **15**, 7098 (2013).
- [35] A. Jorio, M. S. Dresselhaus, R. Saito, and G. Dresselhaus, *Raman Spectroscopy in Graphene Related Systems* (Wiley-VCH, Weinheim, Germany, 2011).
- [36] A. C. Ferrari, and D. M. Basko, Raman spectroscopy as a versatile tool for studying the properties of graphene, *Nat. Nanotechnol.* **8**, 235 (2013).
- [37] R. Saito, Y. Tatsumi, S. Huang, X. Ling, and M. S. Dresselhaus, Raman spectroscopy of transition metal dichalcogenides, *J. Phys. Condens. Matter* **28**, 353002 (2016).
- [38] Xin Zhang, Qing-Hai Tan, Jiang-Bin Wu, Wei Shi, and Ping-Heng Tan, Review on the Raman spectroscopy of different types of layered materials, *Nanoscale* **8**, 6435 (2016).
- [39] M. Huang, H. Yan, C. Chen, D. Song, T. F. Heinz, and J. Hone, Phonon softening and crystallographic orientation of strained graphene studied by Raman spectroscopy, *Proc. Natl. Acad. Sci. USA* **106**, 7304 (2009).
- [40] T. M. G. Mohiuddin, A. Lombardo, R. R. Nair, A. Bonetti, G. Savini, R. Jalil, N. Bonini, D. M. Basko, C. Galiotis, N. Marzari, K. S. Novoselov, A. K. Geim, and A. C. Ferrari, Uniaxial strain in graphene by Raman spectroscopy: g peak splitting, Grüneisen parameters, and sample orientation, *Phys. Rev. B* **79**, 205433 (2009).
- [41] Elena del Corro, Ladislav Kavan, Martin Kalbac, and Otakar Frank, Strain assessment in graphene through the Raman 2D' mode, *J. Phys. Chem. C* **119**, 25651 (2015).
- [42] Y. Wang, C. Cong, C. Qiu, and T. Yu, Raman spectroscopy study of lattice vibration and crystallographic orientation of monolayer MoS₂ under uniaxial strain, *Small* **9**, 2857 (2013).
- [43] H. J. Conley, B. Wang, J. I. Ziegler, R. F. Haglund, Jr., S. T. Pantelides, and K. I. Bolotin, Bandgap engineering of strained monolayer and bilayer MoS₂, *Nano Lett.* **13**, 3626 (2013).
- [44] C. Rice, R. J. Young, R. Zan, U. Bangert, D. Wolverson, T. Georgiou, R. Jalil, and K. S. Novoselov, Raman-scattering measurements and first-principles calculations of strain-induced phonon shifts in monolayer MoS₂, *Phys. Rev. B* **87**, 081307 (2013).
- [45] Hong Li, Alex W. Contryman, Xiaofeng Qian, Sina Moeini Ardakani, Yongji Gong, Xingli Wang, Jeffrey M. Weisse, ChiHwan Lee, Jiheng Zhao, Pulickel M. Ajayan, Ju Li, Hari C. Manoharan, and Xiaolin Zheng, Optoelectronic crystal of artificial atoms in strain-textured molybdenum disulphide, *Nat. Commun.* **6**, 7381 (2015).
- [46] Ruixiang Fei, and Li Yang, Lattice vibrational modes and Raman scattering spectra of strained phosphorene, *Appl. Phys. Lett.* **105**, 083120 (2014).
- [47] Yanyong Li, Zhixin Hu, Shenghuang Lin, Sin Ki Lai, Wei Ji, and Shu Ping Lau, Giant anisotropic raman response of encapsulated ultrathin black phosphorus by uniaxial strain, *Adv. Funct. Mater.* **27**, 1600986 (2017).
- [48] Danna Doratotaj, Jeffrey R. Simpson, and Jia-An Yan, Probing the uniaxial strains in MoS₂ using polarized Raman spectroscopy: A first-principles study, *Phys. Rev. B* **93**, 075401 (2016).
- [49] A. J. Huber, A. Ziegler, T. Köck, and R. Hillenbrand, Infrared nanoscopy of strained semiconductors, *Nat. Nanotechnol.* **4**, 153 (2009).
- [50] P. Hohenberg, and W. Kohn, Inhomogeneous electron gas, *Phys. Rev.* **136**, B864 (1964).
- [51] W. Kohn, and L. J. Sham, Self-consistent equations including exchange and correlation effects, *Phys. Rev.* **140**, A1133 (1965).
- [52] Stefano Baroni, Stefano de Gironcoli, Andrea Dal Corso, and Paolo Giannozzi, Phonons and related crystal properties from density-functional perturbation theory, *Rev. Mod. Phys.* **73**, 515 (2001).
- [53] Thibault Sohier, Matteo Calandra, and Francesco Mauri, Density functional perturbation theory for gated two-dimensional heterostructures: Theoretical developments and application to flexural phonons in graphene, *Phys. Rev. B* **96**, 075448 (2017).
- [54] Paolo Giannozzi, *et al.*, QUANTUM ESPRESSO: A modular and open-source software project for quantum simulations of materials, *J. Phys. Condens. Matter* **21**, 395502 (2009).
- [55] P. Giannozzi, *et al.*, Advanced capabilities for materials modelling with QUANTUM ESPRESSO, *J. Phys. Condens. Matter* **29**, 465901 (2017).

- [56] Hendrik J. Monkhorst, and James D. Pack, Special points for Brillouin-zone integrations, *Phys. Rev. B* **13**, 5188 (1976).
- [57] Thibault Sohier, Marco Gibertini, Matteo Calandra, Francesco Mauri, and Nicola Marzari, Breakdown of optical phonons' splitting in two-dimensional materials, *Nano Lett.* **17**, 3758 (2017).
- [58] Michele Lazzeri, and Francesco Mauri, First-principles calculation of vibrational Raman spectra in large systems: Signature of small rings in crystalline SiO₂, *Phys. Rev. Lett.* **90**, 036401 (2003).
- [59] Dirk Porezag, and Mark R. Pederson, Infrared intensities and Raman-scattering activities within density-functional theory, *Phys. Rev. B* **54**, 7830 (1996).
- [60] J. P. Perdew, and Alex Zunger, Self-interaction correction to density-functional approximations for the many-electron systems, *Phys. Rev. B* **23**, 5048 (1981).
- [61] G. B. Bachelet, D. R. Hamann, and M. Schlüter, Pseudopotentials that work: From H to Pu, *Phys. Rev. B* **26**, 4199 (1982).
- [62] Xavier Gonze, Roland Stumpf, and Matthias Scheffler, Analysis of separable potentials, *Phys. Rev. B* **44**, 8503 (1991).
- [63] Atsushi Togo, Spglib, (accessed: 2016), <https://atztogo.github.io/spglib/>.
- [64] Yoyo Hinuma, Giovanni Pizzi, Yu Kumagai, Fumiyasu Oba, and Isao Tanaka, Band structure diagram paths based on crystallography, *Comput. Mater. Sci.* **128**, 140 (2017).
- [65] T. Hahn ed., *International Tables for Crystallography*, 5th ed., Vol. A: Space-Group Symmetry (Springer, Dordrecht, The Netherlands, 2005).
- [66] E. J. Mele, and Petr Král, Electric polarization of heteropolar nanotubes as a geometric phase, *Phys. Rev. Lett.* **88**, 056803 (2002).
- [67] D. Sánchez-Portal, and E. Hernández, Vibrational properties of single-wall nanotubes and monolayers of hexagonal BN, *Phys. Rev. B* **66**, 235415 (2002).
- [68] Ludger Wirtz, Angel Rubio, Raul Arenal de la Concha, and Annick Loiseau, *Ab initio* calculations of the lattice dynamics of boron nitride nanotubes, *Phys. Rev. B* **68**, 045425 (2003).
- [69] K. H. Michel, and B. Verberck, Phonon dispersions and piezoelectricity in bulk and multilayers of hexagonal boron nitride, *Phys. Rev. B* **83**, 115328 (2011).
- [70] Yecun Wu, Duan Zhang, Kangho Lee, Georg S. Duesberg, Askar Syrlybekov, Xiao Liu, Mourad Abid, Mohamed Abid, Yanqi Liu, Lisheng Zhang, Jiung Cho, Miri Choi, Byong Sun Chun, Haomao Wang, Huajun Liu, and Han-Chun Wu, Quantum confinement and gas sensing of mechanically exfoliated GaSe, *Adv. Mater. Technol.* **2**, 1600197 (2017).
- [71] Dattatray J. Late, Bin Liu, H. S. S. Ramakrishna Matte, C. N. R. Rao, and Vinayak P. Dravid, Rapid characterization of ultrathin layers of chalcogenides on SiO₂/Si substrates, *Adv. Funct. Mater.* **22**, 1894 (2012).
- [72] Thomas E. Beechem, Brian M. Kowalski, Michael T. Brumbach, Anthony E. McDonald, Catalin D. Spataru, Stephen W. Howell, Taisuke Ohta, Jesse A. Pask, and Nikolai G. Kalugin, Oxidation of ultrathin GaSe, *Appl. Phys. Lett.* **107**, 173103 (2015).
- [73] Alaric Bergeron, John Ibrahim, Richard Leonelli, and Sebastien Francoeur, Oxidation dynamics of ultrathin GaSe probed through Raman spectroscopy, *Appl. Phys. Lett.* **110**, 241901 (2017).
- [74] Charalampos Androulidakis, Emmanuel N. Koukaras, John Parthenios, George Kalosakas, Konstantinos Papagelis, and Costas Galiotis, Graphene flakes under controlled biaxial deformation, *Sci. Rep.* **5**, 18219 (2015).
- [75] Fang Liu, Pingbing Ming, and Ju Li, *Ab initio* calculation of ideal strength and phonon instability of graphene under tension, *Phys. Rev. B* **76**, 064120 (2007).
- [76] See Supplemental Material at <http://link.aps.org/supplemental/10.1103/PhysRevApplied.11.024012> for details of the Poisson's-coefficient dependence on strain. The Supplemental Material also contains details of the phonon dispersion under strain onset for lattice instability, geometry deformation under strain, and mechanical stiffness.
- [77] Basant Chitara, and Assaf Ya'akovovitz, Elastic properties and breaking strengths of GaS, GaSe and GaTe nanosheets, *Nanoscale* **10**, 13022 (2018).
- [78] O. H. Nielsen, and Richard M. Martin, Quantum-mechanical theory of stress and force, *Phys. Rev. B* **32**, 3780 (1985).
- [79] O. H. Nielsen, and Richard M. Martin, Stresses in semiconductors: *Ab initio* calculations on Si, Ge, and GaAs, *Phys. Rev. B* **32**, 3792 (1985b).
- [80] O. H. Nielsen, and Richard M. Martin, First-principles calculation of stress, *Phys. Rev. Lett.* **50**, 697 (1983).
- [81] S. Demirci, N. Avazl, E. Durgun, and S. Cahangirov, Structural and electronic properties of monolayer group III monochalcogenides, *Phys. Rev. B* **95**, 115409 (2017).
- [82] Simone Bertolazzi, Jacopo Brivio, and Andras Kis, Stretching and breaking of ultrathin MoS₂, *ACS Nano* **5**, 9703 (2011).
- [83] Changgu Lee, Xiaoding Wei, Jeffrey W. Kysar, and James Hone, Measurement of the elastic properties and intrinsic strength of monolayer graphene, *Science* **321**, 385 (2008).
- [84] R. Longuinhos, and J. Ribeiro-Soares, Ultra-weak inter-layer coupling in two-dimensional gallium selenide, *Phys. Chem. Chem. Phys.* **18**, 25401 (2016).
- [85] G. Grimvall, *Thermophysical Properties of Materials* (Elsevier, Amsterdam, 1999).
- [86] C. Thomsen, S. Reich, and P. Ordejón, *Ab initio* determination of the phonon deformation potentials of graphene, *Phys. Rev. B* **65**, 073403 (2002).
- [87] F. Cerdeira, C. J. Buchenauer, Fred H. Pollak, and Manuel Cardona, Stress-induced shifts of first-order Raman frequencies of diamond- and zinc-blende-type semiconductors, *Phys. Rev. B* **5**, 580 (1972).
- [88] H. Sakata, G. Dresselhaus, M. S. Dresselhaus, and M. Endo, Effect of uniaxial stress on the Raman spectra of graphite fibers, *J. Appl. Phys.* **63**, 2769 (1988).
- [89] Y. C. Cheng, Z. Y. Zhu, G. S. Huang, and U. Schwingenschlögl, Grüneisen parameter of the *g* mode of strained monolayer graphene, *Phys. Rev. B* **83**, 115449 (2011).
- [90] Nicolas Mounet, and Nicola Marzari, First-principles determination of the structural, vibrational and thermodynamic properties of diamond, graphite, and derivatives, *Phys. Rev. B* **71**, 205214 (2005).